crystals

MDPI

Article

Relationships between the Structural, Vibrational, and Optical Properties of Microporous Cancrinite

Roman Shendrik [1], Ekaterina Kaneva [1,2,*], Tatiana Radomskaya [1,2], Igor Sharygin [3] and Alexander Marfin [3]

[1] Vinogradov Institute of Geochemistry, Siberian Branch of the Russian Academy of Sciences, 664033 Irkutsk, Russia; r.shendrik@gmail.com (R.S.); taniaojigova@mail.ru (T.R.)
[2] Department of Subsoil Use, Irkutsk National Research Technical University, 664074 Irkutsk, Russia
[3] Institute of the Earth's Crust, Siberian Branch of the Russian Academy of Sciences, 664033 Irkutsk, Russia; isharygin@crust.irk.ru (I.S.); marfin1309@gmail.com (A.M.)
* Correspondence: kev604@mail.ru

Abstract: The crystal-chemical, vibrational, and optical properties of microporous aluminosilicate cancrinite have been investigated by combining electron probe microanalysis, single-crystal X-ray diffraction, infrared (IR) absorption, Raman, UV-Visible absorption, and electron spin resonance spectroscopy. The behavior of the peaks in the IR spectra was also studied during the dehydration of the sample. The analyzed sample has the following unit cell parameters ($P6_3$): a = 12.63189(14) Å, c = 5.13601(7) Å. The empirical formula, based on 12(Si + Al), is $Na_{6.47}Ca_{1.23}K_{0.01}[Al_{5.97}Si_{6.03}O_{24}](CO_3)_{1.45}(SO_4)_{0.03}Cl_{0.01}\cdot 2H_2O$. The Al-Si framework of AB-type is formed by columns of based-shared "cancrinite" (CAN) cages, containing Na and H_2O positions located on the 3-fold axis, and channels with CO_3 groups, lying in two mutually exclusive and partially occupied positions in the center of the channel, and split Na/Ca cation sites. The revealed characteristics are somewhat different in comparison with the cancrinite structural features previously described in the literature. Studied crystals change color from grayish-pink to blue after X-ray irradiation (10^4 Gy). The blue color of the irradiated cancrinite is caused by the formation $(CO_3)^{-\bullet}$ radicals in the crystals. Combining the results obtained using the selected methods will provide a better understanding of the relationships between the structural, chemical, and optical-physical properties of microporous aluminosilicates.

Keywords: cancrinite; crystal structure; crystal chemistry; IR spectroscopy; Raman spectroscopy; optical absorption spectroscopy; ESR

Citation: Shendrik, R.; Kaneva, E.; Radomskaya, T.; Sharygin, I.; Marfin, A. Relationships between the Structural, Vibrational, and Optical Properties of Microporous Cancrinite. *Crystals* **2021**, *11*, 280. https://doi.org/10.3390/cryst11030280

Academic Editor: Alexey M. Pugachev

Received: 27 February 2021
Accepted: 11 March 2021
Published: 12 March 2021

1. Introduction

Cancrinite is a widespread mineral, having white, light blue, gray, yellowish, greenish, or bright yellow color. Its name corresponds to the surname of Count Georg Ludwig Cancrin, Russian Minister of Finance (XIX century). Cancrinite is an aluminosilicate belonging to the feldspathoid family, characterized by layers of six-membered rings of Si- and Al-tetrahedra stacked along c to form a three-dimensional open-framework. The framework density, defined as the number of framework knots per 1000 Å^3, is equals to 16.9 [1], a value lying in the range (from 14 to 22) found for zeolites and microporous mineral phases. Moreover, the mineral was considered as promising zeolite for accommodating various inorganic and organic species in the structural voids. That it is useful for the development of new pigments [2] and storage tanks containing high-level waste [3].

Cancrinite contains $(CO_3)^{2-}$ as the main anionic component in the channel voids. The ideal chemical formula of cancrinite (according to IMA List of Minerals) can be written as $(Na,Ca,\square)_8(Al_6Si_6)O_{24}](CO_3,SO_4)_2\cdot 2H_2O$.

The crystal structure of cancrinite was first solved by Pauling (1930) [4] and then refined by Jarchow (1965) [5]. To obtain a better understanding of the crystal chemistry of cancrinite-group minerals, electron probe microanalysis (EPMA), single-crystal X-ray

diffraction (SCXRD), and infrared (IR) spectroscopy have been mostly used [6–13]. However, the study of the optical properties has not been carried out; in particular, studies on the origin of the color of the mineral have not been previously reported.

In the present work, a cancrinite sample from Zhidoi alkaline complex (Russia) has been studied using a combination of the following techniques: EPMA, SCXRD, IR and Raman spectroscopy, optical absorption spectroscopy, and electron spin resonance (ESR). The combination of the results coming from the selected techniques is expected to provide further insights into the relationships between the structural, chemical, and physical properties and substitution mechanisms characteristic of microporous aluminosilicates.

2. Materials and Methods

2.1. Sample Description

The studied cancrinite was taken from Zhidoi alkaline complex (Tunka Range, Irkutsk region, Russia), situated in the Southern framing of the Siberian Craton, and mainly composed of silicate rocks with perovskite and ilmenite pyroxenites, dikes of ijolites, nepheline and cancrinite syenites, and carbonatites [14]. Cancrinite is found here in the form of aggregates of prismatic crystals of grayish-pink color up to 3–5 mm in length; it associates with aegirine and nepheline.

2.2. Electron Probe Microanalysis (EPMA)

EPMA data of the same crystal used for single-crystal X-ray diffraction analysis were obtained with a JEOL JXA-8200 electron microprobe (JEOL Ltd., Tokyo, Japan). The analysis was performed in a wavelength-dispersive spectroscopic (WDS) mode with a 15 kV accelerating voltage, 5 nA beam current, and a ~20 μm spot size. The following standards were employed: Pyrope (Si), albite (Al, Na), diopside (Ca), orthoclase (K), ZnS (S), Cl-apatite (Cl). A conversion from X-ray counts to oxide weight percentages (wt.%) was obtained with the ZAF data reduction method.

2.3. Single-Crystal X-ray Diffraction (SCXRD)

X-ray diffraction analysis of the selected single crystal was performed using a Bruker AXS D8 VENTURE automated diffractometer (Bruker, Berlin, Germany) equipped with a Photon 100 detector, and Mo$K\alpha$ radiation. Operating conditions were: 50 kV and 1 mA, crystal-to-detector distance of 40 mm. A set of 24 frames was used for initial cell determination with a strategy optimized by the APEX2 suite package [15]. Complete data collection was then accomplished by several φ and ω scans with 0.3° rotation and 5.5 s exposure time per frame. The half of the Ewald sphere ($\pm h$, $\pm k$, $\pm l$) was recorded in theta ranges up to ~40°. Data reduction was performed using CrysAlisPro Version 1.171.39.46 [16]. Least-squares refinement was performed using the program CRYSTALS [17] in the space group $P6_3$. The refined parameters were scale factor, atom positions, anisotropic displacement parameters, and occupancies for extra framework cations and anions. The relevant details of structure refinement are reported in Table 1. The CIFs were deposited with the Cambridge Crystallographic Data Centre (CCDC 2064244).

Figures showing structural details were prepared using the program VESTA (version 4.3.0) [18].

Table 1. Selected data on single crystal, data collection, and structure refinement parameters of the studied cancrinite sample.

Crystal Data	
a (Å)	12.63189(14)
b (Å)	12.63189(14)
c (Å)	5.13601(7)
V (Å^3)	709.730(17)
Z	1
Crystal dimensions (mm)	0.226 × 0.114 × 0.049
Data Collection	
Independent reflections	2551
$R_{merging}$ [$R_{(int)}$] (%)	2.90
h_{min}, h_{max}	−21, 21
k_{min}, k_{max}	−21, 21
l_{min}, l_{max}	−8, 8
Refinement	
Space group	$P6_3$
Reflections used in the refinement ($I > 3\sigma_{(I)}$)	2402
N. of refined parameters	108
R [a] [on F] (%)	2.97
R_w [b] [on F] (%)	3.01
Goof [c]	1.0899
$\Delta\rho_{min}/\Delta\rho_{max}$ (e$^-$/Å^3)	−0.51/0.58

[a] $R = \Sigma[|F_o| - |F_c|]/\Sigma|F_o|$. [b] $R_w = [\Sigma[w(F_o^2 - F_c^2)^2]/\Sigma[w(F_o^2)^2]]^{1/2}$; w = Chebyshev optimized weights. [c] Goodness-of-fit = $[\Sigma[w(F_o^2 - F_c^2)^2]/(N - p)]^{1/2}$, where N and p are the number of reflections and parameters, respectively.

2.4. Raman and Infrared (IR) Spectroscopy

Raman spectra of randomly oriented cancrinite grains were obtained using a WITec alpha300R confocal Raman spectroscopic system (WITec GmbH, Ulm, Germany) coupled with frequency-doubled 532 nm Nd:YAG laser at room temperature. The spectra were recorded with a diffraction grating 1800 gr mm^{-1} with spectral resolution 3 cm^{-1}. The output power of the laser beam was 15 mW. The diameter of the focal spot on the sample was 5–10 µm. The backscattered Raman signal was collected with a Zeiss 50×/NA 0.55 objective throughput UHTS300 spectrometer equipped with a Peltier-cooled, front-illuminated CCD camera; signal acquisition time for a single scan of the spectral range was 1 s, and the signal was averaged over 100 scans. Crystalline silicon was used as a standard.

In order to obtain IR absorption spectra of the cancrinite, powdered samples were mixed with anhydrous KBr, pelletized, and analyzed using an FT-801 spectrometer (Simex, Novosibirsk, Russia) at a resolution of 1 cm^{-1}. Thirty-two scans were collected for each spectrum. The IR spectrum of an analogous pellet of pure KBr was used as a reference. The dehydration procedure with subsequent IR spectra acquisition is the same as described in [19,20]. The heating rate was 10 K/min.

2.5. Optical Absorption Spectroscopy and Electron Spin Resonance (ESR)

Diffuse-light optical absorption spectra of the cancrinite were measured at room temperature with a PerkinElmer Lambda 950 spectrophotometer (Perkin-Elmer, Shelton, CT, USA) in an integrating sphere. For measurements, the samples were placed in a quartz test tube, which is transparent in the range of 270–830 nm (37,000–12,000 cm^{-1}). The light beam was completely concentrated on the sample [21–23].

Electron spin resonance (ESR) spectra were recorded using a RE-1306 X-band spectrometer (KBST, Smolensk, Russia) with a frequency of 9.257 GHz. Small single crystal grain of the cancrinite was mounted in a quartz dewar in the resonator. A magnetic field

was applied along the *c* axis of the cancrinite. The measurements were carried out at 77 K [23].

Irradiation of the cancrinite samples was performed by an X-ray tube with Pd-anode operated at 40 kV, 20 mA for 30 min (10^4 Gy) at room temperature.

3. Results

3.1. Chemical Composition and Structure Description

Chemical composition results, obtained from 10 analyses, show that the samples examined are relatively homogeneous, particularly regarding Al_2O_3 (29.5–29.9 wt.%), SiO_2 (35.2–35.5 wt.%), Na_2O (19.0–19.9 wt.%), CaO (6.3–6.8 wt.%), K_2O (0.04–0.07 wt.%), SO_3 (0.5–0.7 wt.%), Cl (0–0.08 wt.%) contents (91.7–92.7 wt.% total). The distinctive features of the chemical composition will be considered in detail in the Discussion chapter. CO_2 (3.1–3.4 wt.%) content was calculated from charge balance, H_2O (3.5 wt.%) was derived from stoichiometry. Total sum = 98.3–99.6 wt.%. The presence of CO_3 groups and H_2O molecules was confirmed by infrared (IR) and Raman spectroscopy (see below).

The chemical formula calculated based on 12(Si + Al) atoms per formula unit for studied cancrinite is $Na_{6.47}Ca_{1.23}K_{0.01}[Al_{5.97}Si_{6.03}O_{24}](CO_3)_{1.45}(SO_4)_{0.03}Cl_{0.01}\cdot 2H_2O$.

Final atomic coordinates and displacement parameters are given in Tables 2 and 3, selected interatomic bond distances and angles are listed in Table 4.

Table 2. Crystallographic coordinates, occupancies, and equivalent/isotropic atomic displacement parameters (Å^2) of cancrinite sample.

Site	*x/a*	*y/b*	*z/c*	Occ.	Ueq
Na1	2/3	1/3	0.1268(5)	0.896(10)	0.0323
Na2	0.1270(3)	0.2572(4)	0.2638(10)	0.58(2)	0.0252
Ca2	0.12128(18)	0.2447(2)	0.3048(7)	0.334(14)	0.0181
Si1	0.328382(18)	0.410543(19)	0.7400(3)	1	0.0067
Al2	0.07556(2)	0.41210(2)	0.7406(3)	1	0.0066
O1	0.20328(6)	0.40530(7)	0.6480(3)	1	0.0123
O2	0.11309(8)	0.56252(6)	0.7173(3)	1	0.0182
O3	0.02998(7)	0.34914(7)	0.0494(3)	1	0.0135
O4	0.31364(7)	0.35660(7)	0.0339(3)	1	0.0138
C1	0	0	0.8966(15)	0.378(8)	0.0273
O_{C1}	0.1177(3)	0.0586(4)	0.4071(15)	0.378(8)	0.0614
C2	0	0	0.671(2)	0.472(8)	0.0466
O_{C2}	0.0583(2)	0.1198(2)	0.6628(7)	0.472(8)	0.0380
Ow	2/3	1/3	0.6702(14)	1	0.1893
H1	0.7233	0.4282	0.6408	2/3	0.1053

Table 3. Anisotropic atomic displacement parameters (Å^2) of cancrinite sample.

Site	U11	U22	U33	U23	U13	U12
Na1	0.0195(4)	0.0195(4)	0.0579(10)	0	0	0.0098(2)
Na2	0.0198(7)	0.0417(15)	0.0216(11)	0.0149(9)	0.0070(6)	0.0211(9)
Ca2	0.0169(4)	0.0142(7)	0.0226(8)	0.0008(4)	−0.0005(4)	0.0073(4)
Si1	0.00640(8)	0.00671(8)	0.00722(8)	0.00045(8)	0.00011(8)	0.00355(6)
Al2	0.00599(8)	0.00666(9)	0.00707(9)	0.00036(9)	−0.00003(8)	0.00312(6)
O1	0.0090(2)	0.0196(3)	0.0123(2)	0.0026(2)	0.00100(19)	0.0102(2)
O2	0.0207(3)	0.0111(2)	0.0265(4)	0.0016(3)	0.0020(3)	0.0108(2)
O3	0.0118(3)	0.0208(3)	0.0096(3)	0.0044(2)	0.00294(18)	0.0095(2)
O4	0.0153(3)	0.0223(3)	0.0079(3)	0.0030(2)	0.00109(18)	0.0125(2)
C1	0.0097(11)	0.0097(11)	0.063(4)	0	0	0.0048(6)
O_{C1}	0.0210(16)	0.0303(18)	0.128(6)	−0.010(2)	−0.010(2)	0.0092(13)
C2	0.0174(12)	0.0174(12)	0.105(7)	0	0	0.0087(6)
O_{C2}	0.0176(9)	0.0138(9)	0.082(3)	0.0073(9)	0.0041(10)	0.0076(6)
Ow	0.264(10)	0.264(10)	0.040(2)	0	0	0.132(5)

Table 4. Selected bond distances (Å) and angles (°) of the studied cancrinite sample.

Bond Distances				Angles	
Si1-O1	1.6187(11)	Al2-O1	1.7248(11)	O1-Si1-O2	107.76(4)
Si1-O2	1.6136(6)	Al2-O2	1.7172(8)	O1-Si1-O3	107.14(4)
Si1-O3	1.6316(16)	Al2-O3	1.7382(20)	O1-Si1-O4	110.40(4)
Si1-O4	1.6281(20)	Al2-O4	1.7474(14)	O2-Si1-O3	112.39(5)
<Si1-O>	1.623	<Al2-O>	1.732	O2-Si1-O4	112.45(5)
				O3-Si1-O4	106.59(4)
Na1-O1	2.8606(10)			<O-Si1-O>	109.46
Na1-O1′$^{(\times 2)}$	2.8617(7)	C1-$O_{C1}$$^{(\times 3)}$	1.2887(33)		
Na1-O2$^{(\times 2)}$	2.4546(10)	C2-$O_{C2}$$^{(\times 3)}$	1.3114(22)	O1-Al2-O2	106.76(4)
Na1-O2′	2.4557(12)			O1-Al2-O3	109.45(4)
Na1-Ow	2.3451(76)	Ow-H1	1.055(1)	O1-Al2-O4	106.67(4)
Na1-Ow′	2.7909(76)			O2-Al2-O3	114.50(4)
<Na-O>	2.636			O2-Al2-O4	114.18(4)
				O3-Al2-O4	104.99(3)
(1)		(2)		<O-Al2-O>	109.43
Na2-O1	2.5533(50)	Na2-O1	2.5533(50)		
Na2-O3	2.3424(55)	Na2-O3	2.3424(55)		
Na2-O3′	2.9055(44)	Na2-O3′	2.9055(44)	Si1-O1-Al2	146.69(5)
Na2-O4	2.3598(39)	Na2-O4	2.3598(39)	Si1-O2-Al2	152.78(6)
Na2-O4′	2.9279(52)	Na2-O4′	2.9279(52)	Si1-O3-Al2	133.11(5)
Na2-O_{C1}	2.3845(82)	Na2-O_{C2}	2.4827(61)	Si1-O4-Al2	133.09(5)
Na2-O_{C1}′	2.5364(52)	Na2-O_{C2}′	2.5038(38)		
Na2-O_{C1}″	2.5601(77)	Na2-O_{C2}″	2.5414(58)		
<Na-O>	2.571	<Na-O>	2.577	O_{C1}-C1-$O_{C1}$$^{(\times 3)}$	119.83(8)
				O_{C2}-C1-$O_{C2}$$^{(\times 3)}$	119.90(6)
(1)		(2)			
Ca2-O1	2.4888(32)	Ca2-O1	2.4888(32)		
Ca2-O3	2.5125(34)	Ca2-O3	2.5125(34)	H1-Ow-H1′	118.00(1)
Ca2-O3′	2.8355(27)	Ca2-O3′	2.8355(27)		
Ca2-O4	2.5305(27)	Ca2-O4	2.5305(27)		
Ca2-O4′	2.8729(32)	Ca2-O4′	2.8729(32)		
Ca2-O_{C1}	2.3682(40)	Ca2-O_{C2}	2.2908(45)		
Ca2-O_{C1}′	2.3871(62)	Ca2-O_{C2}′	2.4175(41)	C1-C2	1.159(13)
Ca2-O_{C1}″	2.4704(76)	Ca2-O_{C2}″	2.4434(28)	C1-C2	1.409(13)
<Ca-O>	2.558	<Ca-O>	2.549		

The crystal structure of cancrinite is illustrated in Figure 1. The framework of cancrinite is schematically shown in Figure 2a. It is formed through an *ABAB*...-stacking sequence (AB-type), describing the relative translations of the layers, containing rings of Al- and Si-centered tetrahedra. On the basis of observed <T–O> distances for Si and Al-centered tetrahedra (Table 4), it is possible to state that Si and Al regularly alternate on the T sites. The Si-Al framework contains columns of based-shared "cancrinite" cages (CAN) and channels, formed by 12-membered Al-Si-rings. Cages and channels are connected by distorted 6-membered and 4-membered windows. Cancrinite cage and channel arranged along the *c* axis and will be described separately. The structural cavities and channels host extra-framework alkaline (Na, minor K) and earth-alkaline (Ca) cations, water molecules, carbonate, and minor sulfate and chlorine anionic groups. All Ca was located at the M2 site.

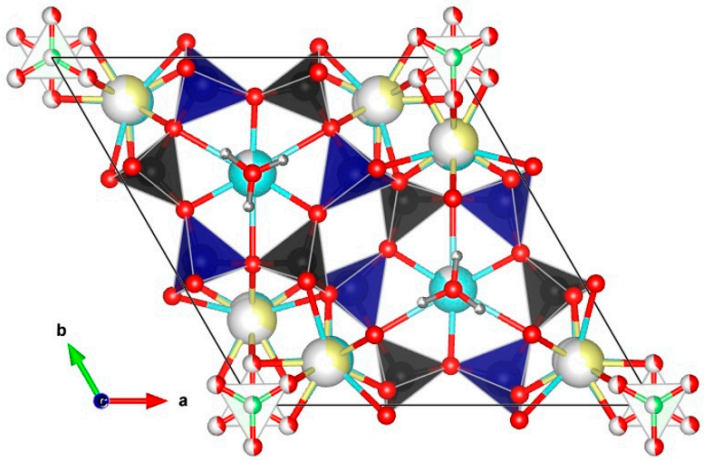

Figure 1. Crystal structure of cancrinite viewed down the *c* axis (single unit cell). Si- and Al-tetrahedra are black and blue, respectively. Na and Ca are cyan and yellow large spheres, respectively; O, C, and H are red, green, and gray small spheres, respectively. The partially white coloring of the spheres indicates a vacancy.

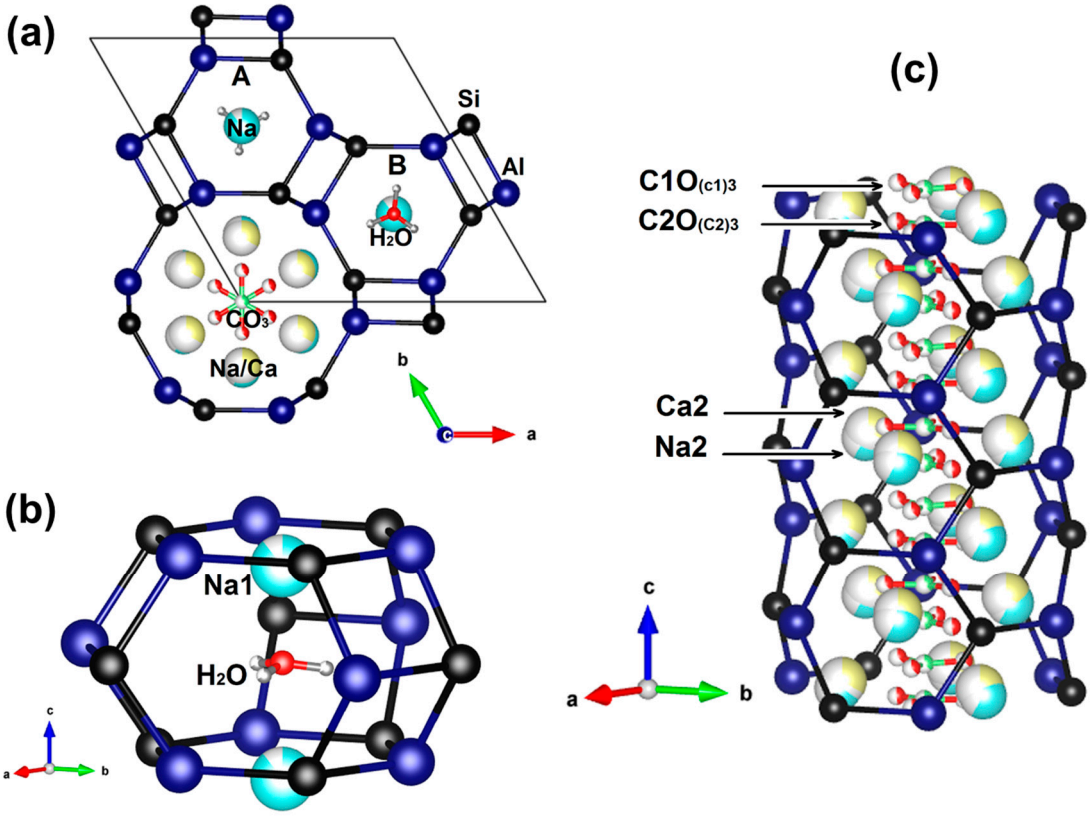

Figure 2. The schematic representation of cancrinite framework (**a**), which consists of CAN cages (**b**) and channels (**c**), occupied by extra framework cations (Na and Ca are cyan and yellow large sphere, respectively), anionic groups (C and O of CO_3 triangles are red and green small spheres, respectively), and water molecules (O and H atoms are red and gray, respectively). The partially white coloring of the spheres indicates a vacancy. An AB-stacking sequence is illustrated (**a**).

3.2. Cancrinite Cage

The cancrinite cage, $[4^6 6^5]$ according to the IUPAC rules [24], has a thickness along the *c* corresponding to two layers. The cage is hendecahedral and composed of six four-membered and five six-membered rings (Figure 2b). In the refined structure, chains of cancrinite cages occur at (1/3, 2/3, *z*) and (2/3, 1/3, *z*) (Figures 1 and 2a). Each CAN cage

contains Na1 and H_2O positions located on the 3-fold axis. The Ow bonded strongly to the Na1 cation on the one side and to a second Na1 cation of neighboring cancrinite cage on another side, with bond distances of 2.345(8) Å and 2.791(8) Å, respectively (Table 4). The H1 position was found to have the statistical distribution of corresponding hydrogen atoms with a probability of 1/3. Ow–H1 distances is 1.055 Å (H1–Ow–H1 angle is 118.0°), the shortest H1···O distance is 2.962(1) Å.

3.3. Channel

The channel (Figure 2c), denoted as $[6^6 12^{2/2}]$ [24], occurs at (00*z*) (Figure 1) and contains CO_3 groups, lying in two mutually exclusive and partially occupied positions in the center of the channel, and cation site, distributed into two split positions: Na2 and Ca2 with occupancies of 0.58 and 0.33, respectively. Carbon atoms in the channel are located over four levels along the *c* axis, with C1-C2 distances of 1.16(1) Å on the one side and 1.41(1) Å on another side, and occupancies equal 0.38 (C1, and the corresponding O_{C1}) and 0.47 (C2, and the corresponding O_{C2}). Sodium and calcium cations inside the channel can be coordinated either by oxygen atoms belonging to triangle $C1O_{(C1)3}$ (case (1) in Table 4), or, in the second case ((2) in Table 4), by oxygens of $C2O_{(C2)3}$ group.

3.4. Raman Spectroscopy

The Raman spectra of initial and irradiated cancrinite are provided in Figure 3. An intense band at 1057 cm^{-1} is assigned to the $(CO_3)^{2-}$ ν_1 symmetric stretching mode. Nakamoto et al. (1957) [25] first published and tabulated the selection rules for $(CO_3)^{2-}$ anions. The free ion, $(CO_3)^{2-}$ with D_{3h} symmetry exhibits four normal vibrational modes; a symmetric stretching vibration (ν_1), an out-of-plane bend (ν_2), a doubly degenerate asymmetric stretch (ν_3) and another doubly degenerate bending mode (ν_4). The symmetries of these modes are A_1'(Raman) + A_2''(IR) + E′(Raman, IR) + E″(Raman, IR) and occur at 1063, 879, 1415, and 680 cm^{-1}, respectively. A second band is observed at 1049 cm^{-1} and is also assigned to this vibrational mode. The structure of cancrinite possesses two non-equivalent positions of $(CO_3)^{2-}$ bonded to both the monovalent and divalent cations. This may lead to two symmetric stretching vibrations.

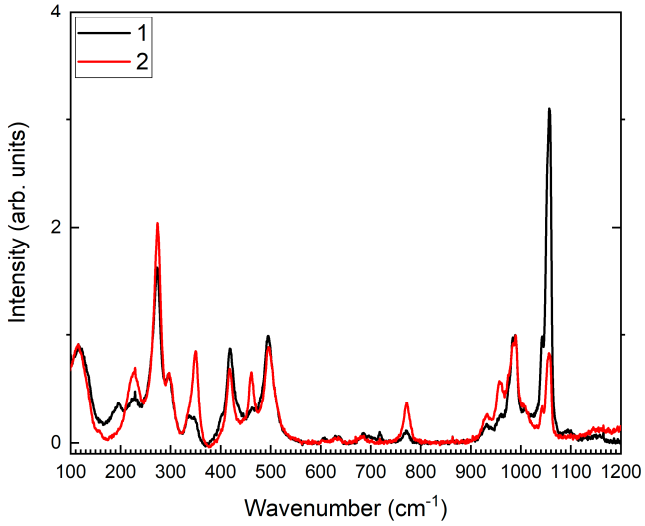

Figure 3. Raman spectra of the cancrinite before (curve 1) and after irradiation (10^4 Gy) (curve 2).

A series of weak bands at 930, 960, 1005, and strong band at 985 cm^{-1} are assigned to antisymmetric alumosilicate framework (T-O-T) stretching vibrations. A weak intensity band at 770 cm^{-1} could represent the inter-tetrahedral symmetric T-O-T stretching vibration [26]. However, in carbonate minerals such as coalingite, brugnatellite a peak in region

760–800 cm^{-1} was assigned to $(CO_3)^{2-}$ ν_4 bending modes [27]. Martins et al. (2017) [28] also involved the 770 cm^{-1} peak to ν_4 bending modes of $(CO_3)^{2-}$ in cancrinite.

Peaks below 500 cm^{-1}: 495, 420, 345, 337, 295, 275, 225, 195, 115 cm^{-1} are interpreted to be deformational modes of the aluminosilicate framework νδO–Si(Al)–O and (Na–Ca)–O modes [26,29]. In the region 3500–3620 cm^{-1} two weak bands peaked at 3540 and 3600 cm^{-1} are attributed to O-H stretching modes of water molecules. This region is not shown in the Figure 3.

3.5. Infrared Spectroscopy

The infrared absorption spectrum of the cancrinite is presented in Figure 4. The spectrum consists of a group of overlapping strong bands of stretching vibrations with absorption peaks in the following spectral regions (a) 980 and 1080 cm^{-1}—stretching vibrations of the aluminosilicate framework; (b) three relatively narrow bands corresponding to mixed vibrations of the framework of tetrahedra (in the ranges 578 cm^{-1}, 621 cm^{-1} and 675–685 cm^{-1}); (c) asymmetric stretch vibrations ν_3 of $(CO_3)^{2-}$ in the range 1360–1590 cm^{-1} and out-of-plane ν_2 $(CO_3)^{2-}$ mode at 855 cm^{-1}; (d) bending vibration at 1628 cm^{-1} and stretching vibration in the range 3000–3800 cm^{-1} of water molecules located in the cancrinite cages [12]. Modes related to $(SO_4)^{2-}$ radicals located at 585 cm^{-1} in Raman [19] and 1160–1180 cm^{-1} in infrared absorption spectra [12] are not observed in the studied cancrinite. Intense mode ν_1 of $(SO_4)^{2-}$ group at 990–1000 cm^{-1} are overlapped with the bands of the aluminosilicate framework, but ν_4 mode located at 585 cm^{-1} in Raman [19] and ν_3 mode 1160–1180 cm^{-1} in infrared absorption spectra [12] are not observed in the studied cancrinite.

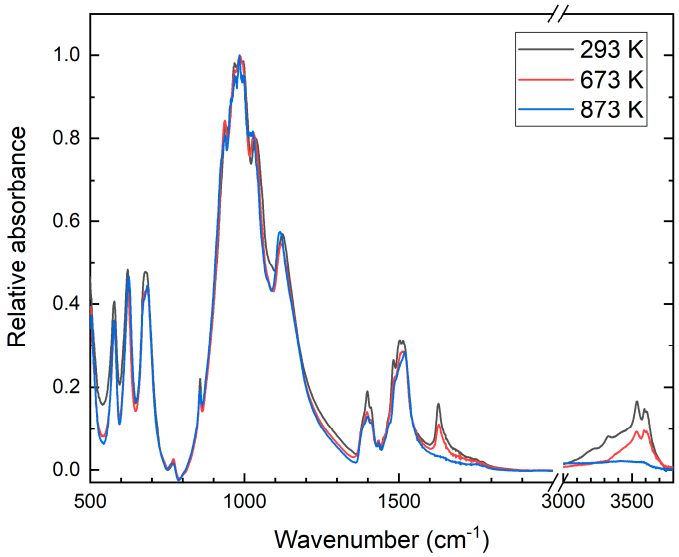

Figure 4. Infrared absorption spectra of the cancrinite before annealing and dehydrated at 673 and 873 K. All spectra were measured at room temperature at the same conditions.

The absorption bands of mixed vibrations of the aluminosilicate framework in the range 570–700 cm^{-1} are sensitive to the spatial structure of feldspathoids. Chukanov et al. (2011) [12] found a correlation between positions of the framework mixed vibration bands and types of the framework in different cancrinites. Samples with an AB-type framework show three distinct bands in this range; changes in the stacking of layers are characterized by an additional splitting of the bands attributed to framework mixed vibrations. In the studied sample, the bands at 578 and 685 cm^{-1} correspond spectra of cancrinite solid-solutions in [12] with AB-type framework that is slightly disturbed by water molecules in structure.

As pointed out above, the carbonate anion $(CO_3)^{2-}$ is the most common carbon-containing extra-framework species in cancrinite minerals. Mostly the anions are planar and have close to D_{3h} symmetry. They have three active modes in an IR absorption spectrum (Figure 4). The most surround sensitive mode is asymmetric stretch vibrations ν_3 of $(CO_3)^{2-}$ in the range 1360–1590 cm^{-1}. This mode is doubly degenerate and it splits into two bands at about 1400 and 1500 cm^{-1}. The band at 1400 cm^{-1} has a slightly resolved structure with peaks at 1385, 1398, 1409, 1434 cm^{-1}. The band at about 1500 cm^{-1} also has a structure with peaks at 1450, 1483, 1503,1515, 1520 cm^{-1}. As it was revealed from structural refinement, in the investigated cancrinite two non-equivalent positions of $(CO_3)^{2-}$ exist. Chukanov et al. (2011) [12] pointed, that the content of Ca in cancrinite was the most important factor in determining splitting and position of the second band related to ν_3 mode. The average position of the second band of ν_3 mode at about 1500 cm^{-1} is usually observed in Ca-rich cancrinite minerals with Ca content 1.19–1.6 apfu. That is in agreement with crystal-chemical data (1.2 apfu). The splitting and position of the second band can be explained by the generation of chain vibrations due to the resonance between ν_3-type vibrations of neighboring $Na_2Ca(CO_3)$ clusters [12].

3.6. Optical Absorption Spectroscopy and ESR

Studied crystals have light grayish-pink color and opaque. Therefore, the optical absorption spectrum is measured in a diffuse light integration sphere. The absorption spectrum of the initial sample is given in Figure 5. Weak absorption bands at about 19,000 (525 nm), 27,600 (360 nm), 30,600 (325 nm), and 35,300 (280 nm) cm^{-1} are found. The ESR signal in the samples is not registered.

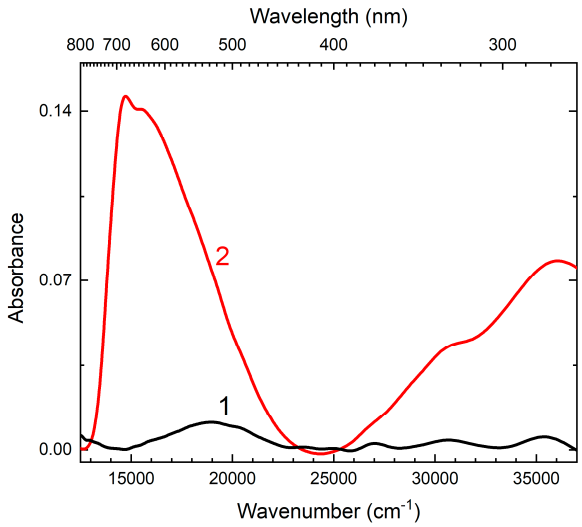

Figure 5. UV-Visible absorption spectrum of the cancrinite before (curve 1) and after (curve 2) irradiation (10^4 Gy).

The irradiated samples become blue color (Figure 6). The absorption spectrum of the irradiated cancrinite is given in Figure 5. Strong bands in the region 12,500–23,900 cm^{-1} (800–435 nm) and 25,000–37,000 cm^{-1} (400–270 nm) appear. The band at 12,500–23,900 cm^{-1} has a slightly resolved structure with peaks at 14,800 and 15,500 cm^{-1} (675 and 645 nm respectively). In addition, an intense ESR signal having $g_{\perp}$=2.015 is registered in the irradiated sample (Figure 7). The intensities of absorption band and ESR signal decrease with the heating of the sample above 400 K and the samples remain initial color and ESR signal disappear at 550 K.

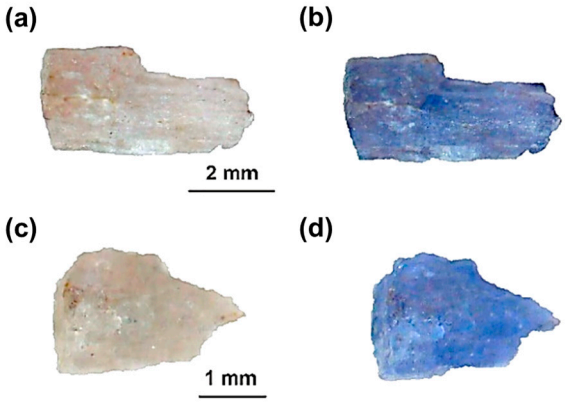

Figure 6. Cancrinite samples: Before (**a**,**c**) and after (**b**,**d**) irradiation (10^4 Gy).

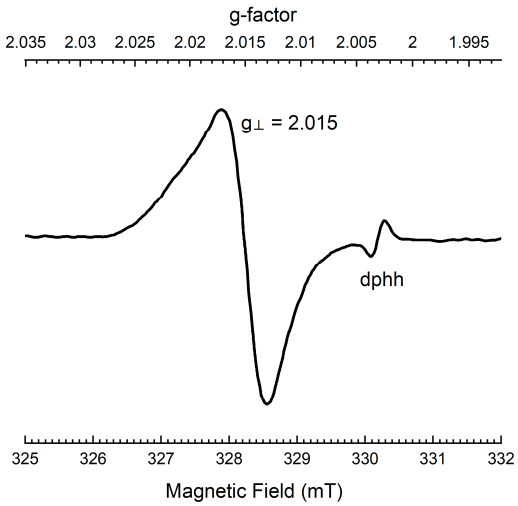

Figure 7. First derivative electron spin resonance (ESR) spectrum of the irradiated (10^4 Gy) cancrinite using a standard marker of dphh (di(phenyl)-(2,4,6-trinitrophenyl)iminoazanium).

Raman spectrum of the irradiated sample is also changed (Figure 3, red curve). Intensities of the ν_1 $(CO_3)^{2-}$ related bands are decreased and the 195 cm^{-1} band is disappeared, but intensities of the 770, 460, and 345 cm^{-1} bands are strongly increased in the irradiated sample. After heating the irradiated sample to 550 K the Raman spectrum becomes the same as before irradiation.

4. Discussion

4.1. Crystal-Chemical Features

The sample selected for the present work has a chemical composition close to most of the previously studied cancrinite minerals. Chemical data, represented in Table 5, show that cancrinite is substantially free of chlorine (~0.03 wt.% Cl), potassium (~0.06 wt.% K_2O), and sulfur (~0.3 wt.% SO_3). The main difference between the chemistry of the reference minerals represented in Table 5 and the studied one is that our cancrinite contains significant amounts of calcium (~6.8 wt.% CaO vs. 0.20–5.32, excluding the sample analyzed by [6]; see Table 5). The structural formulas of the studied sample of cancrinite and those from literature are represented in Table 6. Concerning the chemical composition of the cationic and anionic filling of the "cancrinite" (CAN) cage and the channel, the samples represented in Table 6 do not have particularly large differences. It can be noted that three main structural features of cancrinite are distinguished: (1) Localization of the water molecule (on the third-order axis or outside it); (2) disordering of the CO_3-group into several subpositions (from 2 to 4) and (3) disordering of the cationic position, designated M2, which

in most cases has a mixed occupancy by Na and Ca atoms. Comparing the literature data, one can conclude that the studied sample is close to two cancrinites: A mineral from Ilmeny Mtns (Russia) [30] and a sample from Bancroft (Canada) [31]. However, none of the previously described cancrinite samples have all three structural features similar to studied cancrinite from Zhidoi. In the two mentioned samples of the mineral [30,31], the M2 position is ordered.

Table 5. Chemical data of cancrinite. For comparison purpose, reference data are reported.

	Zhidoi (Russia) This Study	Oktiabrski (Ukraine) [32]	Satom Quarry (Cameroun) [10]	IMC Quarries (Canada) [10]	Khibiny (Russia) [33]	Kovdor (Russia) [9]	Satom Quarry (Canada) [8]	Satom Quarry (Canada) [7]	Bancroft (Canada) [6] †
SiO_2	35.6(3)	39.59(92)	35.62	35.54	38.04	38.39	35.09	37.08	34.35
Al_2O_3	29.9(3)	29.04(50)	29.05	29.50	27.36	29.63	28.47	30.03	29.35
Na_2O	19.7(2)	18.64(61)	19.80	19.71	21.03	24.15	20.37	19.82	17.66
MgO	b.d.l.	n.d.	n.d.	n.d.	n.d.	n.d.	n.d.	n.d.	0.01
K_2O	0.06(5)	0.01(1)	0.03	0.01	0.06	0.25	b.d.l.	b.d.l.	0.10
CaO	6.79(9)	3.55(28)	5.03	5.32	2.99	0.20	4.77	4.72	8.11
MnO	n.d.	0.10(3)	n.d.	n.d.	n.d.	n.d.	n.d.	n.d.	n.d.
Fe_2O_3	n.d.	n.d.	n.d.	n.d.	0.41	0.11	n.d.	n.d.	0.03
Cl	0.03(1)	0.01(1)	0.01	0.03	n.d.	0.07	0.01	b.d.l.	0.21
F	b.d.l.	0.01(2)	0.76	0.04	n.d.	n.d.	b.d.l.	0.50	n.d.
SO_3	0.3(1)	0.02(2)	0.52	0.20	b.d.l.	n.d.	0.52	0.55	n.d.
H_2O	3.54 *	4.00(7) **	3.49 *	3.51 *	4.05*	n.d.	3.43 *	3.50 *	3.13
CO_2	3.13 *	3.00(56) **	4.45 *	5.31 *	5.38*	n.d.	5.60 ***	3.50 ***	6.60
Total	99.01	98.85	98.74	99.19	99.32	93.31	98.26	99.76	99.55

† Wet analysis; * Data calculated from stoichiometric considerations and charge balance; ** Data obtained with TG-QMS methods; *** Calculated following the procedure described in [7]; n.d.—not detected; b.d.l.—below detection limit.

Table 6. Structural data for the studied sample of cancrinite and comparative data for cancrinites from different deposits (literature data).

Deposit	Space Sroup, Unit Cell Parameters: *a*, Å; *c*, Å; *V*, Å^3	CAN Cage Content, Derived from SCXRD	Ow of the H_2O Molecule Placed on the 3-Fold Axis	Channel Content, Derived from SCXRD	Disordering of CO_3-Group (Num. of Positions)	Disordering of M2 (Na2) Site	Ref.
Zhidoi (Russia)	$P6_3$, 12.6319(1); 5.1360(1); 709.73(2)	$Na_{1.79}(H_2O)_{2.00}$	Yes	$Na_{3.48}Ca_{2.00}(CO_3)_{1.70}$	Yes (2)	Yes	This work
Satom Quarry (Cameroun)	$P6_3$, 12.6018(3); 5.1204(2); 704.21(2)	$Na_{1.91}(H_2O)_{0.18}$	No	$Na_{5.36}Ca_{0.64}(CO_3)_{1.63}$	Yes (2)	Yes	[26]
Eifel (Germany)	$P6_3$, 12.6093(1); 5.1221(1); 705.278(16)	$Na_{1.90}(H_2O)_{2.00}$	No	$Na_{4.14}Ca_{1.44}(CO_3)_{1.57}$	Yes (4)	Yes	[34]
Khibiny (Russia)	$P6_3$, 12.607(2); 5.111(1); 703.5(2)	$Na_{2.00}(H_2O)_{2.00}$	No	$Na_{5.50}Ca_{0.40}(CO_3)_{1.50}$	Yes (3)	Yes	[11]
Khibiny (Russia)	$P6_3$, 12.618(2); 5.116(1); 705.4(2)	$Na_{2.00}(H_2O)_{2.00}$	No	$Na_{5.45}Ca_{0.55}(CO_3)_{1.50}$	Yes (4)	Yes	[11]
Kovdor (Russia)	$P6_3$, 12.683(2); 5.190(1); 723.0(2)	$Na_{2.00}(H_2O)_{2.00}$	No	$Na_{4.80}K_{0.30}(CO_3)_{0.90}$	Yes (3)	No	[11]
Kovdor (Russia)	$P6_3$, 12.606(2); 5.118(1); 704.3(2)	$Na_{2.00}(H_2O)_{2.00}$	No	$Na_{5.80}Ca_{0.20}(CO_3)_{1.40}$	Yes (3)	Yes	[11]
Vishnevye Mtns. (Russia)	$P6_3$, 12.627(2); 5.136(1); 709.2(2)	$Na_{2.00}(H_2O)_{2.00}$	No	$Na_{5.00}Ca_{1.00}(CO_3)_{1.70}$	Yes (4)	Yes	[11]
Tamazeght (Morocco)	$P6_3$, 12.625(2); 5.122(1); 707.0(2)	$Na_{2.00}(H_2O)_{2.00}$	No	$Na_{4.30}Ca_{1.20}(CO_3)_{1.40}$	Yes (2)	No	[11]

Table 6. *Cont.*

Deposit	Space Sroup, Unit Cell Parameters: *a*, Å; *c*, Å; *V*, Å^3	CAN Cage Content, Derived from SCXRD	Ow of the H_2O Molecule Placed on the 3-Fold Axis	Channel Content, Derived from SCXRD	Disordering of CO_3-Group (Num. of Positions)	Disordering of M2 (Na2) Site	Ref.
Tamazeght (Morocco)	$P6_3$, 12.618(2); 5.144(1); 709.3(2)	$Na_{2.00}(H_2O)_{2.00}$	No	$Na_{4.60}Ca_{0.90}(CO_3)_{1.50}$	Yes (3)	No	[11]
Dakhuunur (Russia)	$P6_3$, 12.613(1); 5.124(1); 706.0(2)	$Na_{1.60}(H_2O)_{2.00}$	No	$Na_{4.20}Ca_{1.60}(CO_3)_{1.60}$	Yes (2)	Yes	[11]
Ilmeny Mtns (Russia)	$P6_3$, 12.617(2); 5.129(1); 707.1(2)	$Na_{1.80}(H_2O)_{2.00}$	No	$Na_{4.70}Ca_{1.20}(CO_3)_{1.50}$	Yes (4)	Yes	[11]
Ilmeny Mtns (Russia)	$P6_3$, 12.631(3); 5.1320(5); 709.06(8)	$Na_{2.00}(H_2O)_{1.98}$	Yes	$Na_{4.79}Ca_{0.95}(CO_3)_{1.63}$	Yes (2)	No	[30]
Satom Quarry (Cameroun)	$P6_3$, 12.595(5); 5.121(5); 703.5(8)	$Na_{2.00}(H_2O)_{2.16}$	No	$Na_{5.82}Ca_{0.18}(CO_3)_{1.50}$	Yes (2)	No	[10]
IMC Quarries (Canada)	$P6_3$, 12.60(2); 5.121(5); 704.1(17)	$Na_{2.00}(H_2O)_{2.28}$	No	$Na_{5.88}Ca_{0.12}(CO_3)_{1.54}$	Yes (2)	No	[10]
Kovdor (Russia)	$P3$, 12.727(4); 5.186(2); 727.3(4)	$Na_{2.00}(H_2O)_{2.00}$	No	$Na_{5.70}(CO_3)_{0.90}(SO_4)_{0.10}(H2O)_{0.60}$	Yes (4)	Yes	[9]
Bancroft (Canada)	$P6_3$, 12.5906(2); 5.1168(1); 702.45(2)	$Na_{2.00}(H_2O)_{1.60}$	Yes	$Na_{4.02}Ca_{1.50}(CO_3)_{1.52}$	Yes (2)	No	[31]
Satom Quarry (Canada)	$P6_3$, 12.6216(8); 5.1293(4); 707.65(2)	$Na_{2.00}(H_2O)_{2.00}$	No	$Na_{4.91}Ca_{0.89}(CO_3)_{1.34}$ *	Yes (2)	Yes	[8]
Satom Quarry (Canada)	$P6_3$, 12.622(1); 5.128(1); 707.51(2) (powder XRD)	$Na_{2.00}(H_2O)_{2.00}$	-	$Na_{4.3}Ca_{0.90}(CO_3)_2$ *	Yes (2)	No	[7]
Bancroft (Canada)	$P6_3$, 12.590(3); 5.117(1); 702.42(2)	$Na_{2.00}(H_2O)_{2.00}$	No	$Na_{4.02}Ca_{1.50}(CO_3)_{1.52}$	Yes (2)	No	[6]

* derived from EPMA.

Geometric data and distortion parameters for the cancrinite sample are given in Table 7. Analyzing the structural model of cancrinite, several features can be noted. The Al2 site appears to have a valence sum that is too high (3.26 vu), indicating the possibility of partial entry into this position of a more highly charged cation, i.e., Si. The Al2 tetrahedron also displays the higher TAV (16.5480) parameter with respect to Si1 (TAV = 6.9838). The BLD, ELD, and TQE values are similar for Si1 and Al2. For sodium and calcium polyhedra, the distortion parameters are also close.

Table 7. Calculated geometrical and distortion parameters for polyhedra in the crystal structure of the studied cancrinite sample. An effective coordination number (ECoN) and the volume of the coordination polyhedron (Vp) were calculated the program VESTA (version 4.3.0) [18]. Bond valence calculations (BVS) were performed using the parameters by [35]. Bond length distortion (BLD) and edge length distortion (ELD) were calculated according to [36]. Tetrahedral angle variance (TAV) and tetrahedral quadratic elongation (TQE) were calculated according to [37].

	Si1	Al2	Na1	
ECoN	3.997	3.994	5.530	
Vp (Å^3)	2.188	2.650	30.639	
BVS	4.012	3.259	0.964	
BLD (%)	0.422	0.630	7.896	
ELD (%)	1.371	1.940	13.260	
TAV	6.9838	16.5480		
TQE	1.0020	1.0051		
	Na2 (1)	**Na2 (2)**	**Ca2 (1)**	Ca2 (2)
ECoN	6.119	6.219	6.647	6.290
Vp (Å^3)	25.010	26.700	25.010	26.700
BVS	1.113	1.090	1.769	1.834
BLD (%)	6.718	6.589	5.785	5.987
ELD (%)	13.781	11.890	13.781	11.890

However, exceptional values were obtained for some anionic positions. The oversaturation of the O_{C1} and O_{C2} sites, when they coordinate calcium (2.24 and 2.22 vu, respectively), indicates local structural disordering. One or two of the three cation atoms are filled with sodium or one of the three calcium atoms is replaced by a vacancy, which has ~9% occupancy in this Na2/Ca2 position. The anionic CO_3-group position within the channel also has an incomplete occupancy (the vacancy is 15%).

The measure of the strain of the crystal structure is expressed in the global instability index (GII), defined by [38]. Values of the GII < 20% suggest that no or reasonable strain is presented, while values > 20% indicate that structure is so strained as to be unstable [39]. To analyze stability, we considered several models: (1) and (2) sodium occupies Na2 position and bonded to two $C1O_{(C1)3}$ or $C2O_{(C2)3}$ triangles, respectively; (3) and (4) calcium occupies Ca2 positions; (5) and (6) sodium occupies Na2 site and bonded to one $C1O_{(C1)3}$ or $C2O_{(C2)3}$ triangle, respectively; (7) and (8) calcium occupies Ca2 site and bonded to one $C1O_{(C1)3}$ or $C2O_{(C2)3}$ triangle, respectively. Due to the Ca2 position being undersaturated, configurations Ca2 + C1 + V and Ca2 + C2 + V have become extremely strained (GII_{total} = 20.83 and 20.46%, Table 8). Cancrinite shows a significantly increased index for Al2 (25.90%) and low value for Si1 (1.20%), but Na, O, and C are still in the medium range. Although the GII value for C in model 6 increases (24.32%), the index for GII_{total} is getting acceptable (16.57%). In the cancrinite crystal structure, calcium is an unstable position. In case 5, significant local relaxation of Na is noted. The overall stress quantified by the global instability index (GII) significantly varies across the models. Assuming only GII_{total} values, structure models 1–6 can be considered stable (GII_{total} ranges from 13.85 to 16.87%, Table 8). The most relaxed are the models in which sodium occupies Na2 position and bonded to two C;1-carbonate groups or one $C1O_{(C1)3}$ group and vacancy. Stability analysis indicates that the coordination of Na2/Ca2 and the environment of CO_3-triangles is the driving force for the stabilization of the crystal structure model. According to [6,40,41] substitutional or positional ordering (or both) of interframework cations and anions may be the reason for the appearance of a superstructure, which should be destroyed on heating [31].

Table 8. The global instability index (GII, %), calculated for crystal structure models of studied cancrinite. V—vacancy.

	GII (%) Na	GII (%) Ca	GII (%) Si	GII (%) Al	GII (%) C	GII (%) O	GII (%) Total
(1) Na2 + 2C1	8.39	-	1.20	25.90	7.40	14.39	13.85
(2) Na2 + 2C2	6.85	-	1.20	25.90	17.20	17.06	15.98
(3) Ca2 + 2C1	3.60	23.41	1.20	25.90	7.40	17.52	16.87
(4) Ca2 + 2C2	3.60	17.2	1.20	25.90	17.20	17.07	16.60
(5) Na2 + C1 + V	2.73	-	1.20	25.90	10.47	15.03	14.09
(6) Na2 + −C2 + V	3.97	-	1.20	25.90	24.32	16.57	16.57
(7) Ca2 + C1 + V	3.60	48.45	1.20	25.90	10.47	15.09	20.83
(8) Ca2 + −C2 + V	3.60	43.96	1.20	25.90	24.32	15.21	20.46

The CAN cage is built from three types of rings: Two horizontal (perpendicular to the *c* axis) 6-membered rings with aperture dimension of 5.281(1) × 5.281(1) × 5.281(1) Å (*ecw* = 2.58 × 2.58 × 2.58 Å), three lateral 6-membered rings with cross-section diameters of 4.952(2), 4.974(2) and 5.136(2) Å (*ecw* = 2.52 × 2.27 × 2.44 Å) and six 4-membered rings (3.569(1) × 4.181(1) Å, *ecw* = 0.87 × 1.48 Å). The ditrigonality (distortion in the form of compression) of the six-membered rings of the framework is increased in the direction of the *c* axis, and is reflected in an increase in the difference between the angles formed by the triads of neighboring oxygen atoms nearest to the ring center. For instance, for a horizontal ring of the CAN cage, the difference [υ(O1–O2–O1) − ψ(O2–O1–O2)] is 32.4°. In the lateral rings, the ditrigonality is defined as the mean difference between the even and odd angles. The ditrigonality value equals 71.7°.

Channels are extended along the *c*-axis and delimited by 12-membered rings of tetrahedra (Figure 2 a,c). The shortest distances between oppositely located oxygen atoms in the ring are 8.456(1) × 9.232(1) Å. A fundamental characteristic of a channel described the accessibility of the pore system to guest species, is *effective channel width* (*ecw*), which is defined as the distance between oxygen atoms in the smallest *n*-ring or smallest free aperture subtracted by 2.7 Å, when the oxygen ionic radius is assumed to be 1.35 Å. Therefore, *ecw* for the studied cancrinite channel is 5.76 × 6.53 Å, while a minimum *ecw* of 3.2 Å is required to be defined as a microporous mineral [42]. Thus, the channels of cancrinite have larger dimensions with respect to the CAN cage aperture and may comprise large guest atoms and molecular groups.

4.2. Dehydration of Cancrinite

H_2O molecules in the cancrinite cages contain three bands of O–H stretching vibrations in the range of 3000–3620 cm^{-1}, corresponding to relatively weak hydrogen bonds. In absorption spectra (Figure 4), absorption peaks of these bands are located at 3320, 3540, and 3605 cm^{-1}. Della Ventura et al. (2009) [10] found that the 3540 and 3605 cm^{-1} bands in the IR absorption spectrum of cancrinite have the same polarization and correspond to H_2O molecules involved in bifurcated hydrogen bonds. The band at 3320 cm^{-1} may be attributed to H_2O molecules occupying vacant sites in the structural channel.

The dehydration of cancrinite was studied with X-ray diffraction methods by [31,43]. They found that the dehydration of cancrinite occurred in temperature interval 470–850 K. In this study, we monitor the dehydration process using IR absorption spectroscopy. The wide band peaked at about 3320 cm^{-1} begin to decrease at about 400 K and it is completely disappeared at 650 K (Figure 8, curve 1). The intensities of absorption bands at 3540 and 3605 cm^{-1} related to stretching vibrations and 1628 cm^{-1} band belonging to bending vibration of H_2O molecules decrease in the range 400–850 K (Figure 8, curve 2). Therefore, these H_2O molecules are located in the structural cages (CAN-cages), similarly to [10]. However, H_2O molecules related to the 3320 cm^{-1} band could be located in the channels with a larger aperture [12].

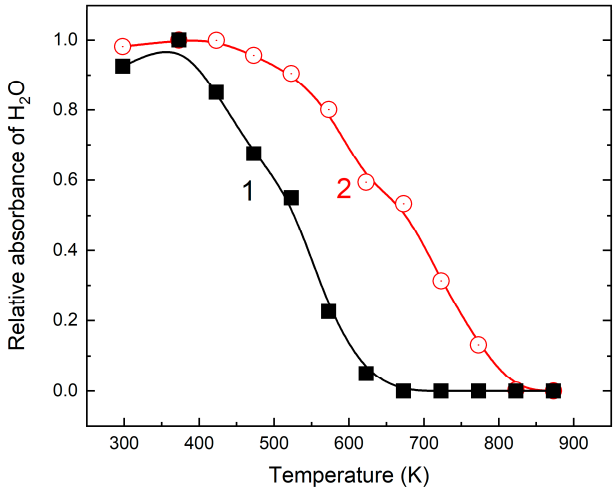

Figure 8. Temperature dependences of the relative intensity of IR absorption at 3200 (curve 1) and 3540 cm^{-1} (curve 2) (stretching vibrations of H_2O molecules).

During the dehydration we find the changing the shape and splitting of the absorption band at about 1500 cm^{-1} attributed to ν_3 of $(CO_3)^{2-}$ mode. The modification of the band in the region 1480–1510 cm^{-1} is started at about 540 K and completed at 850 K together with full dehydration of the cancrinite (Figure 9). The structure of the ν_3 band of dehydrated cancrinite is similar to H_2O-free cancrinite discovered by us in effusive rocks of Bellerberg, Eifel volcanic area, Germany [12]. According to [31], the ordering of the [Ca-CO_3] clusters

and vacancies in the channels is destroyed at 504 °C (781 K). Therefore, the structure of the 1500 cm^{-1} band becomes poor due to the disordering of [Ca–CO_3] clusters and their vacancies.

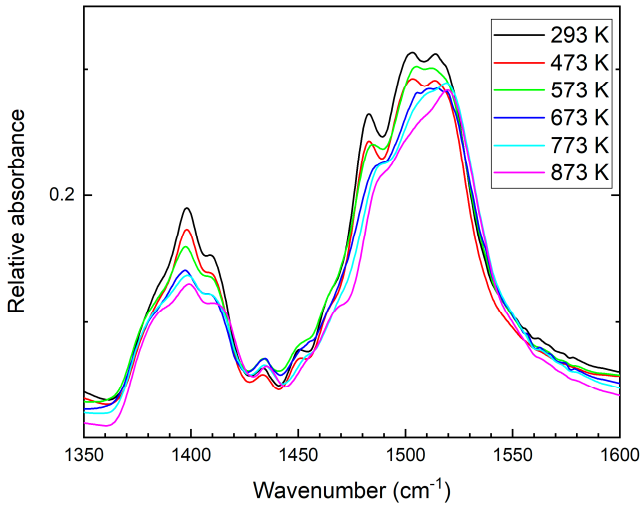

Figure 9. Infrared absorption spectra of the initial (293 K) and dehydrated at 473; 573; 673; 773; and 873 K sample of cancrinite in the spectral region of asymmetric stretch vibrations ν_3. All spectra were recorded at 293 K.

During dehydration positions of two peaks related to aluminosilicate framework vibration modes at 622 and 1036 cm^{-1} are shifted. The maximum of the band at 1036 cm^{-1} is shifted to the lower wavenumbers region at about 10 cm^{-1}, but the peak at 622 cm^{-1} is moved in the opposite direction to 626 cm^{-1} after heating to 700 K. The temperature dependencies of these peak positions are given in Figure 10. The dependences are in agreement with the temperature dependence of angles Si-O4-Al and Si-O3-Al [31], respectively. However, Gatta et al. (2014) pointed that the loss of H_2O at 748 K seems to influence only the Si–O2–Al intertetrahedral angle [43]. Fechtelkord et al. (2001) also showed a decrease in Na1–O1 and a constant Na1–O2 [44]. Furthermore, an inversion of the Si–O2–Al vs. temperature behavior following the dehydration process was pointed out by [30]. Therefore, we can conclude that Al-O2-Si atoms participate in the vibrations with the 622 and 1036 cm^{-1} modes.

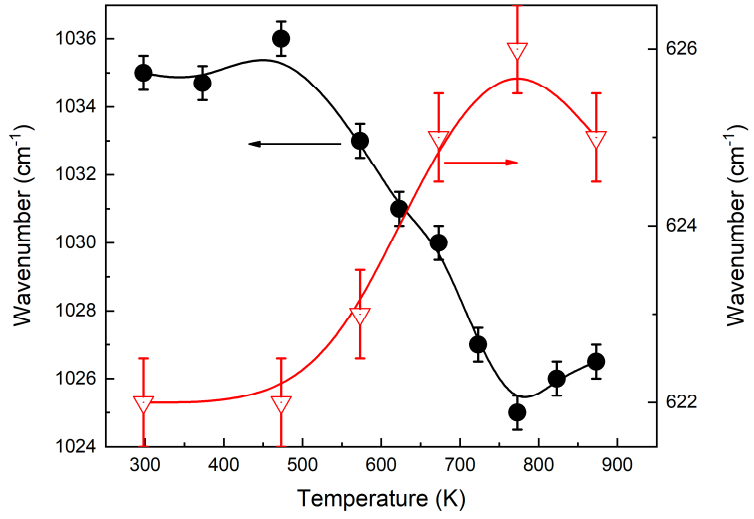

Figure 10. Temperature dependencies of the IR absorption peak positions of the aluminosilicate framework vibration modes.

4.3. Color of Cancrinite

Natural cancrinite very rarely has a blue color. We found only one photography of blue color cancrinite from Farnese, Viterbo Province, Lazio, Italy in the Mindat database (https://www.mindat.org/photo-269943.html). However, the usually blue color of sodalities, lazurites, and kyanoxalite is attributed to the presence of $(S_3)^{-\bullet}$ radicals in cages of the minerals [19,21]. Synthetic cancrinite containing sulfur radicals was studied by [2]. It was found that slightly yellow-blue colored samples contained $(S_3)^{-\bullet}$ radicals and the ESR signal of this radical was registered with g-factor 2.029. In the optical absorption spectrum of synthetic cancrinite, weak intensity structureless band peaked at 629 nm (at about 15900 cm^{-1}) is attributed to transition in $(S_3)^{-\bullet}$ centers. Observed in synthetic cancrinite ESR and optical absorption spectra are close to observed ones in lazurite and sulfur-rich sodalities [19,21], where the wide structureless band peaked at 600 nm and ESR signal with g-factor 2.030 corresponded to $(S_3)^{-\bullet}$ radicals and during heating intensities of $(S_3)^{-\bullet}$ ESR and absorption signal were increased upon heating to 800 K.

Another nature of blue color in carbonate-containing minerals was observed in blue irradiated calcite [45] and Maxixe type beryl [46–48]. The radiation-induced blue color of these minerals was due to the formation of a hole $(CO_3)^{-\bullet}$ radical. The $(CO_3)^{-\bullet}$ radicals demonstrate optical absorption and magnetic circular dichroism in the 12,500–23,900 cm^{-1} spectral region [46,49,50]. In samples containing $(CO_3)^{-\bullet}$ radicals, a strong ESR signal with g-factor 2.016–2.020 is also observed. Therefore, the blue color of irradiated cancrinite is caused by the formation $(CO_3)^{-\bullet}$ radicals in the crystals. A lower energy absorption band could be interpreted as basically a $^2A_2'$–$^2E'$ electron transition, and higher energy absorption band could be attributed to higher energy transition in $(CO_3)^{-\bullet}$ radical from $^2A_2'$ to $^2E''$ state or transitions in vacancy trapped electron centers. The disordering of CO_3 groups yields no vibrational fine structure of the $(CO_3)^{-\bullet}$ absorption band and broadening of the ESR signal.

Changing the Raman spectrum of the irradiated sample requires a more detailed investigation. However, in the region of 418–487 cm^{-1}, antisymmetric modes ν_3 of H_2O-$(CO_3)^{-\bullet}$ radicals are expected [51,52]. On the other hand, the origin of electron traps in cancrinite is unknown. Probably, an electron is captured by a vacancy in the framework, which could also lead to changing some modes of the Raman spectrum.

5. Conclusions

The structural features of cancrinite revealed in this work are unique since they have not previously been found in such a combination among the structural characteristics of cancrinite samples from other localities. In the crystal structure of cancrinite from Zhidoi massif (Russia), the CO_3 groups occupy the center of the channel in two mutually exclusive and iso-oriented configurations. The second characteristic feature of the studied sample is the disordering of the M2 cation position into two sites: Na2 and Ca2. In addition to these two distinctive features, in our sample, Ow position (oxygen of H_2O molecule) is placed on the threefold axis, recently noted only by [30] and [31] for cancrinites from Ilmen Mountains (Russia) and Bancroft (Canada), respectively. Displacement of the Ow from the ideal position at (2/3, 1/3, *z*) was observed in most published structural models (Table 6).

The revealed structural peculiarities are reflected in the position and splitting of characteristic bands associated with vibrations of CO_3 groups in the IR absorption and Raman spectra. The IR absorption spectroscopy was used to clarify the dehydration mechanism, i.e., the releasing of water molecules from structural cages. The mechanism confirmed the previously published results of structural experiments.

Under X-ray irradiation, the cancrinite became blue color. The origin of this color was established by optical spectroscopy and ESR methods. The radiation-induced blue color of the mineral is due to the formation of the hole $(CO_3)^{-\bullet}$ radicals.

Author Contributions: Conceptualization, R.S. and E.K.; methodology, R.S. and E.K.; investigation, R.S., E.K., T.R., I.S., and A.M.; writing—original draft preparation, R.S. and E.K.; visualization, R.S. and E.K. All authors have read and agreed to the published version of the manuscript.

Funding: This research was funded by INRTU, grant number 18-RAS-2020 (Grant of the University Council). The Raman spectroscopic study was supported by the grant No. 075-15-2019-1883 from the Ministry of Science and Higher Education of the Russian Federation.

Institutional Review Board Statement: Not applicable.

Informed Consent Statement: Not applicable.

Data Availability Statement: Not applicable.

Acknowledgments: The authors thank the staff of Sidorov Mineralogical Museum of INRTU, who kindly provided the cancrinite sample studied in this work. The study was carried out using facilities of the Centers for Collective Use: "Center for isotopic-geochemical investigations" at the Vinogradov Institute of Geochemistry SB RAS, "Baikal analytical center for collective use" at the Favorsky Irkutsk Institute of Chemistry SB RAS and the Laboratory of Orogenesis at the Institute of the Earth's Crust SB RAS. We are grateful to reviewers for their valuable comments.

Conflicts of Interest: The authors declare no conflict of interest.

References

1. Baerlocher, C.; McCusker, L.B.; Olson, D.H. *Atlas of Zeolite Framework Types*, 6th ed.; Elsevier: Amsterdam, The Netherlands, 2007.
2. Hoffmann, S.K.; Goslar, J.; Lijewski, S.; Olejniczak, I.; Jankowska, A.; Zeidler, S.; Koperska, N.; Kowalak, S. S^{3-} radicals in ε-cages of cancrinite and zeolite L: Spectroscopic and magnetic resonance studies. *Micropor. Mesopor. Mat.* **2012**, *151*, 70–78. [CrossRef]
3. Buck, E.C.; McNamara, B.K. Precipitation of nitrate-cancrinite in Hanford tank sludge. *Environ. Sci. Technol.* **2004**, *38*, 4432–4438. [CrossRef]
4. Pauling, L. The structure of some sodium and calcium aluminosilicates. *Proc. Natl. Acad. Sci. USA* **1930**, *16*, 453–459. [CrossRef] [PubMed]
5. Jarchow, O. Atomanordnung und strukturverfeinerung von Cancrinit. *Zeitschrift für Kristallographie* **1965**, *122*, 407–422. [CrossRef]
6. Grundy, H.D.; Hassan, I. The crystal structure of a carbonate-rich cancrinite. *Can. Min.* **1982**, *20*, 239–251.
7. Ballirano, P.; Maras, A.; Caminiti, R.; Sadun, C. Carbonate-cancrinite: In-situ real-time thermal processes studied by means of energy-dispersive X-ray powder-diffractometry. *Powder Diffr.* **1995**, *10*, 173–177. [CrossRef]
8. Ballirano, P.; Maras, A. The crystal structure of a "disordered" cancrinite. *Eur. J. Mineral.* **2004**, *16*, 135–141. [CrossRef]
9. Rastsvetaeva, R.K.; Pekov, I.V.; Chukanov, N.V.; Rozenberg, K.A.; Olysych, L.V. Crystal structures of low-symmetry cancrinite and cancrisilite varieties. *Crystallogr. Rep.* **2007**, *52*, 811–818. [CrossRef]
10. Della Ventura, G.; Gatta, G.D.; Redhammer, G.J.; Bellatreccia, F.; Loose, A.; Parodi, G.C. Single-crystal polarized FTIR spectroscopy and neutron diffraction refinement of cancrinite. *Phys. Chem. Minerals* **2009**, *36*, 193–206. [CrossRef]
11. Pekov, I.V.; Olysych, L.V.; Chukanov, N.V.; Zubkova, N.V.; Pushcharovsky, D.Y.; Van, K.V.; Giester, G.; Tillmanns, E. Crystal chemistry of cancrinite-group minerals with an AB-type framework: A review and new data. I. Chemical and structural variations. *Can. Min.* **2011**, *49*, 1129–1150. [CrossRef]
12. Chukanov, N.V.; Pekov, I.V.; Olysych, L.V.; Zubkova, N.V.; Vigasina, M.F. Crystal chemistry of cancrinite-group minerals with an AB-type framework: A review and new data. II. IR spectroscopy and its crystal-chemical implications. *Can. Min.* **2011**, *49*, 1151–1164. [CrossRef]
13. Bonaccorsi, E.; Merlino, S. Modular microporous minerals: Cancrinite-davyne groups and C-S-H phases. *Rev. Mineral. Geochem.* **2005**, *57*, 241–290. [CrossRef]
14. Yarmolyuk, V.V.; Kovalenko, V.I.; Sal'nikova, E.B.; Nikiforov, A.V.; Kotov, A.B.; Vladykin, N.V. Late Riphean rifting and breakup of Laurasia: Data on geochronological studies of ultramafic alkaline complexes in the southern framing of the Siberian Craton. *Doklady Earth Sci.* **2005**, *404*, 1031–1036.
15. *Bruker APEX2*, version 2.0-2; Bruker AXS Inc.: Madison, WI, USA, 2007.
16. *CrysAlisPro Software system*, version 1.171.39.46; Rigaku Oxford Diffraction: Tokyo, Japan, 2018.
17. Betteridge, P.W.; Carruthers, J.R.; Cooper, R.I.; Prout, K.; Watkin, D.J. Crystals version 12: Software for guided crystal structure analysis. *J. App. Cryst.* **2003**, *36*, 1487. [CrossRef]
18. Momma, K.; Izumi, F. VESTA 3 for three-dimensional visualization of crystal, volumetric and morphology data. *J. Appl. Crystallogr.* **2011**, *44*, 1272–1276. [CrossRef]
19. Sapozhnikov, A.N.; Tauson, V.L.; Lipko, S.V.; Shendrik, R.Y.; Levitskii, V.I.; Suvorova, L.F.; Chukanov, N.V.; Vigasina, M.F. On the crystal chemistry of sulfur-rich lazurite, ideally $Na_7Ca(Al_6Si_6O_{24})(SO_4)(S_3)^-$ nH_2O. *Am. Min.* **2021**, *106*, 226–234. [CrossRef]
20. Kaneva, E.; Bogdanov, A.; Shendrik, R. Structural and vibrational properties of agrellite. *Sci. Rep.* **2020**, *10*, 15569. [CrossRef]
21. Chukanov, N.V.; Sapozhnikov, A.N.; Shendrik, R.Y.; Vigasina, M.F.; Steudel, R. Spectroscopic and crystal-chemical features of sodalite-group minerals from gem lazurite deposits. *Minerals* **2020**, *10*, 1042. [CrossRef]

22. Kaneva, E.V.; Shendrik, R.; Radomskaya, T.A.; Suvorova, L.F. Fedorite from Murun alkaline complex (Russia): Spectroscopy and crystal chemical features. *Minerals* **2020**, *10*, 702. [CrossRef]
23. Kaneva, E.; Shendrik, R.; Mesto, E.; Bogdanov, A.; Vladykin, N. Spectroscopy and crystal chemical properties of NaCa2[Si4O10]F natural agrellite with tubular structure. *Chem. Phys. Lett.* **2020**, *738*, 136868. [CrossRef]
24. McCusker, L.B.; Liebau, F.; Engelhardt, G. Nomenclature of structural and compositional characteristics of ordered microporous and mesoporous materials with inorganic hosts (IUPAC Reccomendations 2001). *Pure Appl. Chem.* **2001**, *73*, 381–394. [CrossRef]
25. Nakamoto, K.; Fujita, J.; Tanaka, S.; Kobayashi, M. Infrared spectra of metallic complexes. IV. Comparison of the infrared spectra of unidentate and bidentate metallic complexes. *J. Am. Chem. Soc.* **1957**, *79*, 4904–4908. [CrossRef]
26. Gatta, G.D.; Lotti, P.; Kahlenberg, V.; Haefeker, U. The low-temperature behavior of cancrinite: An in situ single-crystal X-ray diffraction study. *Min. Mag.* **2012**, *76*, 933–948. [CrossRef]
27. Frost, R.L.; Bahfenne, S. Raman and mid-IR spectroscopic study of the magnesium carbonate minerals—Brugnatellite and coalingite. *J. Raman Spectrosc.* **2009**, *40*, 360–365. [CrossRef]
28. Martins, T.; Kressall, R.; Medici, L.; Chakhmouradian, A.R. Cancrinite–vishnevite solid solution from Cinder Lake (Manitoba, Canada): Crystal chemistry and implications for alkaline igneous rocks. *Min. Mag.* **2017**, *81*, 1261–1277. [CrossRef]
29. Reshetnyak, N.B.; Sosedko, T.A.; Tret'yakova, L.I. Combination light scattering in minerals. *Mineral. Zh.* **1988**, *10*, 69–73.
30. Isupova, D.; Ida, A.; Kihara, K.; Morishita, T.; Bulka, G. Asymmetric thermal vibrations of atoms and pyroelectricity in cancrinite. *J. Mineral. Petrol. Sci.* **2010**, *105*, 29–41. [CrossRef]
31. Hassan, I.; Antao, S.M.; Parise, J.B. Cancrinite: Crystal structure, phase transitions, and dehydration behavior with temperature. *Amer. Min.* **2006**, *91*, 1117–1124. [CrossRef]
32. Dumanska-Słowik, M.; Pieczka, A.; Heflik, W.; Sikorska, M. Cancrinite from nepheline syenite (mariupolite) of the Oktiabski massif, SE Ukraine, and its growth history. *Spectrochimica Acta A Mol. Biomol. Spectrosc.* **2016**, *157*, 211–219. [CrossRef]
33. Ogorodova, L.P.; Mel'chakova, L.V.; Vigasina, M.F.; Olysych, L.V.; Pekov, I.V. Cancrinite and cancrisilite in the Khibina-Lovozero alkaline complex: Thermochemical and thermal data. *Geochem. Int.* **2019**, *47*, 260–267. [CrossRef]
34. Zubkova, N.V.; Chukanov, N.V.; Pekov, I.V.; Pushcharovskii, D.Y. Low-hydrous cancrinite: Atomic structure and indicative importance. *Doklady Earth Sci.* **2011**, *439*, 998–1001. [CrossRef]
35. Gagnè, O.C.; Hawthorne, F.C. Comprehensive derivation of bond-valence parameters for ion pairs involving oxygen. *Acta Crystallographica* **2015**, *B71*, 562–578. [CrossRef] [PubMed]
36. Robinson, K.; Gibbs, G.V.; Ribbe, P.H. Quadratic elongation: A quantitative measure of distortion in coordination polyhedra. *Science* **1971**, *172*, 567–570. [CrossRef]
37. Renner, B.; Lehmann, G. Correlation of angular and bond length distortions in TO_4 units in crystals. *Zeitschrift für Kristallographie* **1986**, *175*, 43–59. [CrossRef]
38. Salinas-Sanchez, A.; Garcia-Mucoz, J.L.; Rodriguez-Carvajal, J.; Saez-Puche, R.; Martinez, J.L. Structural characterization of *R*2BaCuO5 (*R* = Y, Lu, Yb, Tm, Er, Ho, Dy, Gd, Eu and Sm) oxides by X-ray and neutron diffraction. *J. Solid State Chem.* **1992**, *100*, 201–211. [CrossRef]
39. Brown, I.D. *The Chemical Bond in Inorganic Chemistry: The Bond Valence Model*; Oxford University Press: Oxford, UK, 2006. [CrossRef]
40. Foit, F.; Peacor, D.; Heinrich, E.W. Cancrinite with a new superstructure from Bancroft, Ontario. *Can. Min.* **1973**, *11*, 940–951.
41. Hassan, I.; Buseck, P.R. The origin of the superstructure and modulations in cancrinite. *Can. Min.* **1992**, *30*, 49–59.
42. Cadoni, M.; Ferraris, G. Synthesis and crystal structure of $Na_2MnSi_4O_{10}$: Relationship with the manaksite group. *Rendiconti Lincei* **2011**, *22*, 225. [CrossRef]
43. Gatta, G.D.; Comboni, D.; Alvaro, M.; Lotti, P.; Cámara, F.; Domeneghetti, M.C. Thermoelastic behavior and dehydration process of cancrinite. *Phys. Chem. Miner.* **2014**, *41*, 373–386. [CrossRef]
44. Fechtelkord, M.; Stief, F.; Buhl, J.-C. Sodium cation dynamics in nitrate cancrinite: A low and high temperature 23Na and 1H MAS NMR study and high temperature Rietveld structure refinement. *Amer. Min.* **2001**, *86*, 165–175. [CrossRef]
45. Serway, R.A.; Marshall, S.A. Electron spin resonance absorption spectrum of orthorhombic CO_3^- molecule-ions in irradiated single crystal calcite. *J. Chem. Phys.* **1967**, *47*, 868–869. [CrossRef]
46. Edgar, A.; Vance, E.R. Electron paramagnetic resonance, optical absorption, and magnetic circular dichroism studies of the CO^-_3 molecular-ion in irradiated natural beryl. *Phys. Chem. Minerals* **1977**, *1*, 165–178. [CrossRef]
47. Mittani, J.C.R.; Watanabe, S.; Chubaci, J.F.D.; Matsuoka, M.; Baptista, D.L.; Zawislak, F.C. γ-radiation effects on colourless silicates of beryl. *Nucl. Instrum. Methods Phys. Res. B* **2002**, *191*, 281–284. [CrossRef]
48. Andersson, L.O. Comments on beryl colors and on other observations regarding iron-containing beryls. *Can. Min.* **2019**, *57*, 551–566. [CrossRef]
49. Figueroa, J.D.; Fuentes-Lemus, E.; Dorta, E.; Melin, V.; Cortés-Ríos, J.; Faúndez, M.; Contreras, D.; Denicola, A.; Álvarez, B.; Davies, M.J.; et al. Quantification of carbonate radical formation by the bicarbonate-dependent peroxidase activity of superoxide dismutase 1 using pyrogallol red bleaching. *Redox Biol.* **2019**, *24*, 101207. [CrossRef] [PubMed]
50. Chantry, G.W.; Horsfield, A.; Morton, J.R.; Whiffen, D.H. The structure, electron resonance and optical spectra of trapped CO_3^- and NO_3. *Mol. Phys.* **1962**, *5*, 589–599. [CrossRef]

51. Tavender, S.M.; Johnson, S.A.; Balsom, D.; Parker, A.W.; Bisby, R.H. The carbonate $(CO_3)^-$ in solution studied by resonance Raman spectroscopy. *Laser Chem.* **1999**, *19*, 056589. [CrossRef]
52. Shkrob, I.A. Ionic species in pulse radiolysis of supercritical carbon dioxide. 2. Ab initio studies on the structure and optical properties of $(CO_2)^{n+}$, $(CO_2)^{2-}$, and $CO_3{}^-$ ions. *J. Phys. Chem. A* **2002**, *106*, 11871–11881. [CrossRef]